

Theory of Drop Formation

Jens Eggers

Universität Gesamthochschule Essen, Fachbereich Physik,
45117 Essen, Germany

We consider the motion of an axisymmetric column of Navier-Stokes fluid with a free surface. Due to surface tension, the thickness of the fluid neck goes to zero in finite time. After the singularity, the fluid consists of two halves, which constitute a unique continuation of the Navier-Stokes equation through the singular point. We calculate the asymptotic solutions of the Navier-Stokes equation, both before and after the singularity. The solutions have scaling form, characterized by universal exponents as well as universal scaling functions, which we compute without adjustable parameters.

I. INTRODUCTION

The breakup of free-surface flows has been an object of intense research from the advent of hydrodynamic theory, and in particular the discovery of surface tension [1–3]. Namely, surface tension is the driving force behind this phenomenon, as it tends to reduce the surface area by decreasing the radius of a column of fluid. This indeed leads to the formation of drops, as is seen most clearly from Rayleigh’s [4] stability analysis of an infinite cylinder of fluid with radius r_0 .

He considered perturbations of different wavelengths and calculated their growth rates. While long wavelength perturbations result in the smallest surface area, they require large mass transport between maxima and minima. Both effects strike a balance at the wavelength $\lambda \approx 9r_0$, corresponding to the fastest growing mode. This type of analysis subsequently has been greatly refined, for example including viscosity [5], surface charges [6], or higher order nonlinear effects [7].

However, even higher order perturbation theory rapidly becomes inadequate as the thickness of the fluid neck goes to zero at a point, and fluid is expelled from this region with increasingly high speed. Near the singularity, characterized by a blow-up of local curvature, and of the velocity at the pinch-point, nonlinear effects will soon dominate the dynamics. An asymptotic scaling theory of this singularity, where surface tension, viscous, and inertial forces are balanced, has been presented very recently [8].

But eventually the size of the neck or the times scale on which it is moving will reach microscopic scales, and a hydrodynamic description breaks down altogether. For example, the neck will evaporate somewhere close to the pinch point, where it has minimum thickness. Shortly after that, new surfaces will have formed on either side, and this time the dynamics is described by two separate Navier-Stokes problems. The physical question we address here is whether the new initial conditions depend on the microscopic mechanisms behind the breakup. In other words, taking two different kinds of fluids with the same surface tension, density, and viscosity, will the breakup look the same on scales larger than the microscopic ones?

We will indeed show that drop formation is a hydrodynamic phenomenon in the above sense. Namely, we construct asymptotic solutions to the Navier-Stokes equation after breakup, which describe two separate surfaces and which are unique continuations of the solutions before breakup. The physical origin of this uniqueness lies in the properties of the solution before breakup [8]. The diameter of the fluid neck does not go to zero uniformly, but only inside a “hot” region around the pinch point. Outside, the solution is static on the time scale of the central region. As one approaches the singularity, the size of the hot region goes to zero. Hence by the time microscopic mechanisms become important, their action is confined to an extremely small region in space. The continuation is achieved by matching the outer parts of the solution before breakup onto the corresponding regions after breakup. Since the outer parts are virtually unaffected by the microscopic dynamics, this procedure yields universal continuations.

This seems to be the first example of a partial differential equation uniquely describing a “topological transition” [9]. The result is also important for numerical simulations, which usually rely on some ad-hoc prescription for the formation of a new surface [10,11], or for breakup in related physical situations [12].

Our paper is organized as follows: In Section 2 we derive a one-dimensional approximation of the Navier-Stokes equation [13,14], valid as the ratio ϵ of the radial to the longitudinal scale of the flow is small. They have self-similar pinching solutions, which are described by a pair of scaling functions $\phi(\xi)$ and $\psi(\xi)$ for the radius of the fluid neck and the velocity, respectively. As the time distance from the singularity goes to zero, the slenderness parameter ϵ for this solution vanishes, making it an exact solution asymptotically.

The scaling functions ϕ and ψ obey two pairs of ordinary differential equations, one for the time before breakup, the other for the time after breakup. For most of the rest of this paper, we will be constructing unique solutions to those equations. In the third section we consider the similarity equations before breakup. Shortly before the singularity, the fluid far outside the pinch region is no longer able to follow the motion near the pinch point. This leads to boundary conditions for the similarity functions at infinity, and together with a regularity condition in the interior, a unique solution of the equations is selected. We compute this solution numerically.

The same procedure is adopted in the fourth section for the similarity equations after breakup. Here the solution is matched onto the profiles before breakup. This solution has two halves, each of which is fixed uniquely by the matching.

The concluding discussion gives an example for the breakup of a real fluid, which could be measured experimentally. We also supply numerical evidence for the uniqueness and stability of our theoretical predictions, and discuss related work.

II. SIMILARITY EQUATIONS

Let us begin by formulating the Navier-Stokes problem for an axisymmetric column of fluid, where we assume the azimuthal velocity to be zero. A sketch of the geometry of the problem can be found in Figure 1. For a fluid with kinematic viscosity ν , surface tension γ , and density ρ the Navier-Stokes equation reads in cylindrical coordinates [15]:

$$\partial_t v_r + v_r \partial_r v_r + v_z \partial_z v_r = -\partial_r p / \rho + \nu(\partial_r^2 v_r + \partial_z^2 v_r + \partial_r v_r / r - v_r / r^2), \quad (1)$$

$$\partial_t v_z + v_r \partial_r v_z + v_z \partial_z v_z = -\partial_z p / \rho + \nu(\partial_r^2 v_z + \partial_z^2 v_z + \partial_r v_z / r) - g, \quad (2)$$

with the continuity equation

$$\partial_r v_r + \partial_z v_z + v_r / r = 0. \quad (3)$$

The acceleration of gravity points in negative z-direction. Here v_z is the velocity along the axis, v_r the velocity in the radial direction, and p the pressure. There are two boundary conditions, coming from the balance of normal forces,

$$\mathbf{n} \cdot \boldsymbol{\sigma} \cdot \mathbf{n} = -\gamma(1/R_1 + 1/R_2), \quad (4)$$

and tangential forces

$$\mathbf{n} \cdot \boldsymbol{\sigma} \cdot \mathbf{t} = 0. \quad (5)$$

In (4),(5) we denoted the outward normal and tangent vector to the surface by \mathbf{n} and \mathbf{t} , $\boldsymbol{\sigma}$ is the stress tensor, and $(1/R_1 + 1/R_2)/2$ the mean curvature. A standard formula for bodies of revolution gives

$$\frac{1}{R_1} + \frac{1}{R_2} = \frac{1}{H(1 + (\partial_z H)^2)^{1/2}} - \frac{\partial_z^2 H}{(1 + (\partial_z H)^2)^{3/2}}, \quad (6)$$

where $H(z, t)$ is the radius of the fluid neck, as seen in Figure 1. The equation of motion for $H(z, t)$ is

$$\partial_t H + v_z \partial_z H = v_r|_{r=H}, \quad (7)$$

which says that the surface moves with the fluid at the boundary.

Equations (1)-(7) constitute a complex moving boundary value problem, which we want to investigate near a singularity, where nonlinear effects are bound to become dominant. The reason exact solutions, valid arbitrarily close to the singularity, can nevertheless be found, is that only very few terms in the equations contribute to the leading order force balance. Thus to proceed, we first have to identify those leading order terms. We will then construct explicit solutions to the leading order equations and demonstrate their consistency with both the internal structure of the Navier-Stokes equation and with boundary conditions.

The relevant terms are identified using two properties of the singularity to be validated later:

- (i) The singularity is line-like, i. e. its axial extension is much greater than its radial extension.
- (ii) Surface tension, viscous, and inertial forces are equally important near the singularity.

Conditions (i) and (ii) are now incorporated into a perturbation theory. According to (i) we will assume that the motion of the fluid at a given time is characterized by an axial length scale ℓ_z and a radial length scale ℓ_r , for which

$$\ell_r = \epsilon \ell_z, \quad (8)$$

where ϵ is some small parameter. The physical meaning of ϵ will come out later from the description of the singularity. Also introducing a time scale t_z of the singularity, we can nondimensionalize all quantities according to

$$\begin{aligned} r &= \ell_r \tilde{r} \quad , \quad z = \ell_z \tilde{z} \quad , \quad t = t_z \tilde{t} \quad , \\ H &= \ell_r \tilde{H} \quad , \quad \mathbf{v} = \frac{\ell_z}{t_z} \tilde{\mathbf{v}} \quad , \quad \frac{p}{\rho} = \frac{\ell_z^2}{t_z^2} \frac{\tilde{p}}{\tilde{\rho}} \quad , \\ \nu &= \frac{\ell_z^2}{t_z} \epsilon^n \tilde{\nu} \quad , \quad \frac{\gamma}{\rho} = \frac{\ell_z^3}{t_z^2} \epsilon^m \frac{\tilde{\gamma}}{\tilde{\rho}} \quad , \quad g = \frac{\ell_z}{t_z^2} \epsilon^l \tilde{g} \quad . \end{aligned} \quad (9)$$

The scales ℓ_z , ℓ_r , and t_z are defined to be constants, so their derivative with respect to time is zero. However, one must bear in mind that the characteristic scales of the singularity change, so ℓ_z , ℓ_r , and t_z will be different in different stages of the singularity formation. Since there are two length scales ℓ_z and ℓ_r , there is a certain freedom in the nondimensionalization of the material parameters ν , γ/ρ , and g . This freedom is completely specified by the exponents n , m , and l in (9). We will see below that the exponents are fixed by the requirement (ii).

Since the radial extension of the fluid is small, we can expand all fields in the dimensionless radial variable \tilde{r} :

$$\tilde{v}_z(\tilde{z}, \tilde{r}, \tilde{t}) = \sum_{j=0}^{\infty} \tilde{v}_{2j}(\tilde{z}, \tilde{t}) (\epsilon \tilde{r})^{2j} \quad , \quad (10)$$

$$\tilde{v}_r(\tilde{z}, \tilde{r}, \tilde{t}) = - \sum_{j=0}^{\infty} \frac{\tilde{v}'_{2j}(\tilde{z}, \tilde{t})}{2j+2} (\epsilon \tilde{r})^{2j+1} \quad , \quad (11)$$

and

$$\tilde{p}(\tilde{z}, \tilde{r}, \tilde{t}) = \sum_{j=0}^{\infty} \tilde{p}_{2j}(\tilde{z}, \tilde{t}) (\epsilon \tilde{r})^{2j} \quad . \quad (12)$$

The definition of \tilde{v}_r automatically ensures incompressibility. We now insert (9)-(12) into the equations of motion (1)-(7), and compare powers in ϵ . The lowest order expressions result in a closed set of equations for \tilde{v}_0 and \tilde{H} ,

$$\partial_{\tilde{t}} \tilde{v}_0 + \tilde{v}_0 \partial_{\tilde{z}} \tilde{v}_0 = -\frac{\tilde{\gamma}}{\tilde{\rho}} \epsilon^{m-1} \partial_{\tilde{z}} \left(\frac{1}{\tilde{H}} \right) + 3\tilde{\nu} \epsilon^n \frac{\partial_{\tilde{z}} \left[(\partial_{\tilde{z}} \tilde{v}_0) \tilde{H}^2 \right]}{\tilde{H}^2} - \tilde{g} \epsilon^l \quad , \quad (13)$$

$$\partial_{\tilde{t}} \tilde{H} + \tilde{v}_0 \partial_{\tilde{z}} \tilde{H} = -(\partial_{\tilde{z}} \tilde{v}_0) \tilde{H} / 2 \quad . \quad (14)$$

To obtain closure at higher orders in ϵ , one needs to expand each of the coefficients \tilde{v}_{2j} and \tilde{p}_{2j} , as well as \tilde{H} into a separate power series in ϵ . There then exists a consistent representation of (1)-(7) to all orders in ϵ [16]. We will not be concerned with the explicit form of the higher order equations here, so for simplicity we use the notation v_0 and H (or its nondimensional counterpart) for the lowest order terms in the expansion in ϵ .

It is evident from (13) that the exponents m , n , and l determine the balance of forces at leading order. Since the $1/\tilde{H}$ term, which comes from the radius of curvature perpendicular to the axis, is driving the instability, it must clearly be present and in fact becomes infinite at the singularity. At the small scales involved in singularity formation, viscosity will also be important. Finally, velocities are expected to blow up as ever smaller amounts of liquid are driven by increasingly large pressure gradients. Hence we also expect inertial effects to be involved asymptotically. Since the acceleration of the fluid diverges at the pinch point, the constant acceleration of gravity will drop out of the problem. This is precisely the assumption (ii), incorporated by choosing $m = 1$, $n = 0$, and $l > 0$ in (9), which leads to an equation where surface tension, viscous, and inertial forces are balanced, while gravity is irrelevant. These assumptions will be tested for consistency later.

We now identify the scales involved in the formation of the singularity. It is crucial to notice that all *external* length and time scales, which are imposed by boundary and initial conditions, do not enter the description of the singularity. In a jet experiment, for example, external scales would be the radius of the nozzle and the period of the driving frequency.

Near the singularity, the length scales characterizing the solution become arbitrarily small, while time scales become shorter and shorter as one approaches the singularity. Hence the singularity moves on scales widely separated from the external scales. It is for this reason that for the mathematical analysis of the singularity we do not have to make the boundary or initial conditions explicit. Boundary and initial conditions will become important when we describe numerical simulations of real experiments, which confirm the consistency of our approach.

The proper units in which to represent the motion near the singularity can thus involve only *internal* parameters of the fluid. This leaves us with the units of length and time

$$\ell_\nu = (\rho \nu^2) / \gamma \quad , \quad t_\nu = (\rho^2 \nu^3) / \gamma^2 \quad . \quad (15)$$

Assuming that the singularity occurs at a point z_0 , and at a time t_0 , the space and time distance from the singularity is properly measured as

$$\begin{aligned} z' &= (z - z_0)/\ell_\nu \quad , \\ t' &= (t - t_0)/t_\nu \quad . \end{aligned} \tag{16}$$

The units ℓ_ν and t_ν are a measure of the width of the critical region, and are fixed for a given fluid. Singular behavior is expected for $|z'| \ll 1$ and $|t'| \ll 1$. Note the conceptual difference to the characteristic scales ℓ_z , ℓ_r , and t_z of the singularity, which change in time.

In the variables z' and t' , the fluid velocity and the neck radius are:

$$\begin{aligned} v(z', t') &\equiv \frac{t_\nu}{\ell_\nu} v_0(z, t) \quad , \\ h(z', t') &\equiv \ell_\nu^{-1} H(z, t) \quad . \end{aligned} \tag{17}$$

Keeping the same terms as in (13),(14) with $m = 1$, $n = 0$, and $l > 0$, we find in the limit $\epsilon \rightarrow 0$

$$\partial_{t'} v + v \partial_{z'} v = -\partial_{z'} \left(\frac{1}{h} \right) + 3 \frac{\partial_{z'} [(\partial_{z'} v) h^2]}{h^2} \quad , \tag{18}$$

$$\partial_{t'} h + v \partial_{z'} h = -(\partial_{z'} v) h / 2 \quad . \tag{19}$$

All material parameters have dropped out of the equations, since everything has been expressed in units of ℓ_ν and t_ν .

At this point it is worthwhile to pause and notice that we have already succeeded in reducing the original Navier-Stokes problem in two spatial dimensions and in time with a moving boundary to just a coupled set of equations in one space dimension and time, at least for small ϵ . Approximations for thin liquid threads of the type described here have in fact a long history, see [13] for a (by no means complete) list of earlier references. However it seems that (18),(19), which contain the correct surface tension, inertial, and viscous terms, were first derived in [13]. Another related approach goes by the name of Cosserat equations, see for example [17]. In all previous work except [8] though, the resulting one- dimensional equations are treated as model equations, whose quality of approximation depends on the particular physical situation for which they are used. In the present paper, we will show that (18), (19) become *exact* close to pinch-off.

To this end we have to identify the parameter ϵ . From the definitions (15) we find

$$t_z/t_\nu = \epsilon^2 \frac{\tilde{\gamma}^2}{\tilde{\rho}^2 \tilde{\nu}^3} \quad , \quad \ell_z/\ell_\nu = \epsilon \frac{\tilde{\gamma}}{\tilde{\rho} \tilde{\nu}^2} \quad . \tag{20}$$

Thus up to constants ϵ^2 is the characteristic time scale of the singularity, written in units of t_ν . But the only such time scale is the nondimensional time distance from the singularity $|t'|$ itself. Hence $|t'|$ serves as the desired smallness parameter. We introduced the modulus of t' here, since we need a measure of the time distance before and *after* the singularity. As $|t'| \rightarrow 0$, all higher order terms vanish and only the leading order equations (18),(19) remain. By the same token, the axial and radial length scales behave like $\ell_z \sim \ell_\nu |t'|^{1/2}$ and $\ell_r \sim \ell_\nu |t'|$. Thus close to the singularity, all length scales become arbitrarily small compared to any external length scale, just as we asserted above.

As a corollary to this absence of any fixed length scale in the problem, we expect singular solutions to have the similarity form

$$\begin{aligned} h &= |t'|^{\alpha_1} \phi(\xi) \quad , \\ v &= |t'|^{\alpha_2} \psi(\xi) \quad , \end{aligned} \tag{21}$$

where the similarity variable ξ is defined as $\xi = z'/|t'|^\beta$. A similar ansatz has been used in [18] for a study of inviscid flow, but in a different geometry.

The values of the exponents α_1 , α_2 , and β are inferred immediately from dimensional analysis. Namely $\ell_r \sim \ell_\nu |t'|$ implies $\alpha_1 = 1$, $\ell_z/t_z \sim (\ell_\nu/t_\nu) |t'|^{-1/2}$ is a typical velocity scale, giving $\alpha_2 = -1/2$, and $\beta = 1/2$ follows from $\ell_z \sim \ell_\nu |t'|^{1/2}$. The appearance of fractional powers forces us to use the modulus of t' in the scaling laws (21). The type of similarity solutions we are going to investigate is thus

$$\begin{aligned}
h &= |t'| \phi(\xi) \quad , \\
v &= \pm |t'|^{-1/2} \psi(\xi) \quad , \\
\xi &= \pm z' / |t'|^{1/2} \quad .
\end{aligned} \tag{22}$$

The two different signs take care of identical solutions with different parity. The acceleration of the fluid diverges like $|t'|^{-3/2}$, and surface tension, viscous, and inertial forces are balanced. Since $|t'| \sim \epsilon^2$ we conclude that the exponent l in (9) is $l = 3$, which is consistent with our previous assumptions.

Inserting (22) into (18) and (19) we find that the asymptotic equations of motion indeed have scaling solutions, where the scaling functions ϕ and ψ obey the equations

$$s(\psi/2 + \xi\psi'/2) + \psi\psi' = \phi'/\phi^2 + 3\psi'' + 6\psi'\phi'/\phi \quad , \tag{23}$$

$$s(-\phi + \xi\phi'/2) + \psi\phi' = -\psi'\phi/2 \quad . \tag{24}$$

The prime refers to differentiation with respect to ξ . The terms in brackets come from the time derivative, $s = 1$ refers to the time before the singularity ($t < t_0$), $s = -1$ to the time after the singularity ($t > t_0$).

Hence close to the singularity, $|t'| \ll 1$ and $|z'| \ll 1$, we have further reduced the problem to a set of two *ordinary differential equations*. To find unique solutions of (23) and (24) we still need to formulate appropriate boundary conditions. This and the numerical integration of (23),(24) will be the subject of the next two sections, first for $t < t_0$, and then for $t > t_0$.

III. BEFORE BREAKUP

In this section we consider the similarity equations (23), (24) for $s = 1$, i.e. before breakup. Some of the calculations relevant for the next section will be done for general s . We show that the similarity equations have precisely one physically allowed solution, and compute it. Therefore singular solutions are completely universal: once the origins of the space and time axes are fixed by specifying z_0 and t_0 , there are no more free parameters. The relevant units of length and time are set by the fluid parameters.

As the similarity equations are of first order in ϕ and of second order in ψ , solutions are specified by three initial conditions $\phi(\xi_i)$, $\psi(\xi_i)$, and $\psi'(\xi_i)$ at a reference point ξ_i . Universality implies that we need to find three conditions which uniquely fix the physically allowed solution.

For the first condition, suppose we choose a small region of width $\ell_\nu \delta$ around the singularity, such that $\delta \ll \min(1, L/\ell_\nu)$, where L characterizes some outer length scale. For $|z'| \leq \delta$ and $|t'| \ll 1$ we are well within the critical region of the singularity, and effects of the boundaries are negligible. Thus the similarity equations (23),(24) apply for $|z'| \approx \delta$ and we have $|t'| \phi(\pm \delta |t'|^{-1/2}) \approx h(\pm \delta, t')$. First we observe that the point $|z'| = \delta$ goes to infinity in similarity variables as $|t'| \rightarrow 0$. Second, in this limit h at $|z'| = \delta$ will not be able to follow the motion of the singularity, whose width decreases like $|t'|^{1/2}$, and whose time scale goes to zero with $|t'|$. Hence $h(\pm \delta, t')$ must approach a finite value as $|t'| \rightarrow 0$. To be consistent with this physical requirement, $\phi(\xi)$ must grow quadratically as $|\xi|$ goes to infinity.

Hence we have two conditions on the solutions of (23),(24):

- a) $\phi(\xi)$, $\psi(\xi)$ need to be regular on the real axis $\xi \in]-\infty, +\infty[$.
- b) For $\xi \rightarrow \pm\infty$, $\phi(\xi)/\xi^2$ should approach a finite limiting value.

Conditions similar to b) have also been employed in [19]. Note that the physical concept behind our argument is inertia, which prohibits the large amount of fluid far away from the singularity to move with the fluid in the skinny pinch region.

We will now show that the requirements a) and b) completely determine the solution of the similarity equations. In particular, we do not have to specify the limiting values of $\phi(\xi)/\xi^2$, they rather come out of the solution of the problem. This is consistent because in our analysis we deal exclusively with the equations of motion valid close to the singularity. No input from regions where the expansion is not valid is needed. Thus boundary or initial conditions can enter the problem only implicitly, as they determine the position of the singularity z_0, t_0 .

Let us begin by examining the behavior of solutions for $\xi \rightarrow \pm\infty$. It is advantageous to first eliminate ϕ from the problem, leaving us with a third-order equation for ψ [20]. To this end (24) is written as

$$\phi' = \phi \frac{s - \psi'/2}{\psi + s\xi/2}. \quad (25)$$

On one hand this equation can be used to express ϕ in terms of ψ ,

$$\phi = [(I' - 3\psi'')/K - 6\psi']^{-1}, \quad (26)$$

where we have introduced the notation

$$\begin{aligned} K &= (s - \psi'/2)/(\psi + s\xi/2) \quad , \\ I &= (s\xi\psi + \psi^2)/2 \quad . \end{aligned} \quad (27)$$

On the other hand, writing ψ as an integral over the kernel K we have

$$\phi = \phi(\xi_0) \exp \left\{ \int_{\xi_0}^{\xi} K(\zeta) d\zeta \right\} \quad .$$

Inserting this into (26), taking the logarithm, and differentiating, we find

$$\psi''' = \frac{K}{3} \{ (I'/K)' + I' + 3\psi''(K'/K^2 - 3) - 6\psi'K \}, \quad (28)$$

which is a single equation just in terms of ψ .

Plugging the ansatz $\psi = B\xi^\alpha$ into (28), one finds the leading order behavior on the right hand side to be

$$\frac{2B}{3\xi} \left[\frac{(\alpha+1)^2}{4} \xi^\alpha + \frac{\alpha+1}{2} \xi^\alpha \right] \quad .$$

Thus ψ must decay like $1/\xi$ or $1/\xi^3$ at infinity for the terms to cancel. In particular, growth of ψ at infinity is prohibited, since the “inertial” term I' is quadratic in ψ , and would grow faster than any other term in (28).

Thus one is lead to an asymptotic expansion of the form

$$\psi = \frac{1}{\xi} \sum_{i=0}^{\infty} b_i \xi^{-2i} \quad . \quad (29)$$

Only odd powers appear, since (28) is invariant under the transformation $\xi \rightarrow -\xi$ and $\psi \rightarrow -\psi$. Using (26) we can calculate the leading behavior of ϕ corresponding to (29):

$$\begin{aligned} \phi &= a_0 \xi^2 [1 + O(\xi^{-2})] \quad , \\ a_0 &= 2/[6b_0 - sb_1 - b_0^2] \quad . \end{aligned} \quad (30)$$

This means (29) represents precisely the physically relevant solutions we are interested in. To further investigate the expansion (29), we derive recursion relations for the coefficients b_i to arbitrarily high order. The lowest order expressions are

$$\begin{aligned} b_2 &= -\frac{1}{2}[3b_0^3 + 7sb_0b_1] \quad , \\ b_3 &= \frac{s}{8}[-30b_0^3 + 9b_0^4 - 148sb_0b_1 - 9sb_0^2b_1 - 10b_1^2 - 8b_2(10 + 3b_0)] \quad . \end{aligned} \quad (31)$$

All b_i are thus determined by just two free coefficients, b_0 and b_1 , or by virtue of (30), a_0 and b_0 . However, the expansion (29) is only asymptotic, as for large i the b_i grow like

$$b_i \sim (-12)^i i! \quad .$$

This means for large ξ all solutions of (28) are *up to exponentially small corrections* given by a two- parameter family of functions $\psi_{a_0 b_0}(\xi)$ [21], which behave like $1/\xi$ asymptotically. The expansion (29) is asymptotic to $\psi_{a_0 b_0}(\xi)$

and for sufficiently large ξ can be used to compute $\psi_{a_0 b_0}(\xi)$ to any desired accuracy. To understand the significance of this observation, we have to investigate the stability of the functions $\psi_{a_0 b_0}(\xi)$.

Doing so turns out to be slightly more convenient in the original space of initial conditions $(\phi(\bar{\xi}), \psi(\bar{\xi}), \psi'(\bar{\xi}))$, where $\bar{\xi} \gg 1$ is kept fixed. Denoting by $\phi_{ab}(\xi)$ the function ϕ corresponding to $\psi_{ab}(\xi)$, we are interested in particular in perturbations which carry us out of the two-dimensional manifold of initial conditions $(\phi_{ab}(\bar{\xi}), \psi_{ab}(\bar{\xi}), \psi'_{ab}(\bar{\xi}))$. Differentiating with respect to a and b , we find that to leading order in $\bar{\xi}$, $(0, 0, 1)$ is a vector normal to this manifold.

We now consider small perturbations relative to the solutions ϕ_{ab}, ψ_{ab} :

$$\begin{aligned}\phi(\xi) &= \phi_{ab}(\xi)(1 + \epsilon_1(\xi)) \\ \psi(\xi) &= \psi_{ab}(\xi)(1 + \epsilon_2(\xi)) \\ \psi'(\xi) &= \psi'_{ab}(\xi)(1 + \epsilon_3(\xi)).\end{aligned}\tag{32}$$

The correction $\epsilon_3(\xi)$ describes the behavior of perturbations perpendicular to the plane of asymptotic solutions $\phi \sim \xi^2$, $\psi \sim \xi^{-1}$. Inserting (32) into (23), (24) and linearizing in the ϵ_i reveals that to leading order ϵ_3 behaves like

$$\epsilon_3(\xi) = \epsilon_3(\bar{\xi}) \exp \left\{ \frac{s\bar{\xi}}{6} (\xi - \bar{\xi}) \right\} \quad .\tag{33}$$

Hence for $s = 1$ an arbitrarily small perturbation introduced at $\bar{\xi}$ will carry the solution away from the physically relevant manifold as $|\xi| \rightarrow \infty$. Only a two-dimensional manifold of solutions is consistent with $\phi(\xi)/\xi^2 \rightarrow \text{const}$ as ξ tends to $+\infty$ or $-\infty$. This means the requirement b) corresponds to *two* constraints on physically relevant solutions. Since the equations are of third order, we need to find one additional constraint to uniquely fix the allowed solutions. It is worth remarking that the unstable growth (33) comes from the presence of the viscous term ψ'' in (23). Hence in a strictly inviscid theory no selection would take place.

To find the third constraint we look at condition a), saying that ϕ, ψ be regular. Considering (25) this is a nontrivial condition, as ψ must be bounded and hence there is a point ξ_0 with

$$\psi(\xi_0) + \xi_0/2 = 0 \quad .\tag{34}$$

Therefore, since $s = 1$, the denominator in (25) will vanish at ξ_0 , leading to a singularity unless the condition

$$\psi'(\xi_0) = 2\tag{35}$$

is also met. To explore the corresponding regular solutions, we expand ψ around ξ_0 :

$$\psi(\xi) = \sum_{i=0}^{\infty} d_i (\xi - \xi_0)^i \quad .\tag{36}$$

The function ϕ can again be recovered from (26). We find

$$\begin{aligned}d_0 &= -\xi_0/2 \quad , \\ d_1 &= 2 \quad , \\ d_2 &= -\frac{5\xi_0}{8(3 - 1/\phi_0)} \quad , \\ d_3 &= \frac{(104 - 1656\phi_0)d_2^2/75 + 6\phi_0}{2 - 36\phi_0} \quad ,\end{aligned}\tag{37}$$

where the first two equations follow from (34) and (35). Just as in the expansion around $\xi = \pm\infty$, all coefficients d_i are determined by only two coefficients, ξ_0 and $\phi_0 = \phi(\xi_0)$. We verified this statement by deriving recursion relations for the d_i to arbitrarily high order. This time the expansion has a finite radius of convergence, whose value depends on the initial conditions ξ_0, ϕ_0 .

It is worthwhile to comment on the physical significance of ξ_0 . The equation of motion for the position z'_s of a marker on the surface h is

$$\partial_t z'_s(t) = v(z'_s(t), t) \quad .\tag{38}$$

Rewriting z'_s in similarity variables, $\xi_s = |t'|^{-1/2} z'_s$, and measuring time on a logarithmic scale, $s = -\ln |t'|$, we find

$$\partial_s \xi_s(s) = \xi_s/2 + \psi(\xi_s) \quad , \quad (39)$$

which is the convection equation in similarity variables. Hence at the point ξ_0 , as defined by (34), a surface marker on ϕ is at rest. Regularity properties on such “stagnation” or “sonic” [22] points often play a similar role in selection.

To explicitly compute the unique solution of the similarity equations before breakup, consistent with a) and b), we proceed as follows: we choose a pair (ξ_0, ϕ_0) and compute the Taylor coefficients d_i to sufficiently high order. This leaves us with a series representation of ψ in a disk around ξ_0 . From there onwards, (28) has to be integrated numerically. Since as $|\xi| \rightarrow \infty$ solutions must be exponentially close to a two-parameter family of functions ψ_{ab} which are “repellent”, solutions will generically not extend to infinity, but rather end up in a singularity at finite ξ . Dominant balance [21] in (28) reveals that those singularities have the leading behavior $\psi(\xi) \sim (\xi - \bar{\xi})^{-1}$. Only a one-dimensional submanifold in (ξ_0, ϕ_0) is consistent with the solution extending to either $+\infty$ or $-\infty$. The point (ξ_0, ϕ_0) where both cross corresponds to the unique solution we are interested in.

Our numerical procedure was to introduce ξ^+ and ξ^- as the values of $|\xi|$ where $|\psi(\xi)|$ exceeded a certain bound as $\xi \rightarrow \infty$ or $\xi \rightarrow -\infty$, respectively. We then optimized ξ_0 and ϕ_0 to give maximum values of ξ^+ and ξ^- . As solutions deviate exponentially from ψ_{ab} , the “window” around $(\bar{\xi}_0, \bar{\phi}_0)$, which allows for solutions extending up to a given $|\xi|$ gets small very rapidly with $|\xi|$. Thus this method allows for a very accurate determination of $\bar{\xi}_0$ and $\bar{\phi}_0$. The numerical values we found are quoted, together with other characteristics of the solution, in Table 1. These results, with the inclusion of the asymptotic expansion (29), now allows us to plot the scaling functions before breakup, ϕ^+ and ψ^+ , in Figure 2.

As seen in Table 1, the stagnation point ξ_0 is extremely close to the point ξ_{min} where ϕ^+ is minimum. This means that in the frame of reference of the surface, fluid is expelled on either side of the minimum. From $z'_{min} = |t'|^{1/2} \xi_{min}$ one sees that the minimum moves with velocity $v_{min} = (\xi_{min}/2)|t'|^{-1/2}$.

To make contact with the qualitative description of the singularity given in the Introduction, we schematically divide the similarity solutions into three regions: A central region around the minimum of size $\xi_{central}$, say, where ϕ is almost constant, and outer regions on either side, where ϕ is quadratic. In this simplified picture, in physical space there is a region of size $\xi_{central}|t'|^{1/2}$ around z_0 , where the diameter of the neck decreases linearly in time, and the velocity diverges like $|t'|^{-1/2}$. Outside this region, both the thickness of the fluid neck and the velocity field are constant. Hence as $|t'| \rightarrow 0$, at any given point $z \neq z_0$ the solution will become static, and the singularity only occurs at a point z_0 in space. In terms of some microscopic length ℓ_{micro} , one can estimate (molecular) mechanisms to be important in a region of size $\xi_{central}(\ell_{micro}\ell_\nu)^{1/2}$.

But perhaps the most striking feature is the extreme asymmetry of ϕ^+ and ψ^+ . Indeed, the values of a_0^\pm , describing the amplitude of ϕ^+ as $\xi \rightarrow \pm\infty$, differ by almost four orders of magnitude. Intuitively, an asymmetric solution is to be expected [14]. Namely, pressure will be higher in the slender part of the solution, pushing fluid over to the right. This will cause the right side of the solution to fill up with even more fluid and get steeper. Eventually, this mechanism is only checked by viscosity. But this argument does not even give an order-of-magnitude estimate of a_0^+/a_0^- . So clearly there is the need for a fully analytical theory of the selection problem, which gives at least reasonable estimates for the numbers in Table 1.

Another, perhaps related problem pertains to the uniqueness of the above solution. In principle, the one-dimensional submanifolds corresponding to the correct asymptotic behavior as $\xi \rightarrow +\infty$ and $\xi \rightarrow -\infty$ could have several crossings, giving a discrete family of solutions. The most reasonable guess for a different form of solution would be a symmetric one, which would then be highly unstable, since small asymmetries would amplify according to the above mechanism. Since $\xi_0 = 0$ for such a solution, ϕ_0 would be the only free parameter, which needs to be consistent with the behavior at infinity. We carefully looked for solutions of this type, but found none. Therefore, to the best of our knowledge, there is precisely one possible solution, but for a final word we must await a rigorous mathematical theory.

IV. AFTER BREAKUP

We now turn to times $t > t_0$, i.e. after breakup. In terms of the similarity equations (23),(24) this means we have to put $s = -1$. But apart from the difference in the equations, there is a completely new type of problem occurring now, related to the mathematical description of a receding tip.

To understand this, let us consider the asymptotic equations (18),(19), which contain the leading order terms of the Navier-Stokes equation as the slenderness parameter ϵ goes to zero. But this description breaks down as one reaches the tip, which is assumed to be at $z'_{tip}(t)$, see Figure 3. Namely, the slenderness assumption means that $\partial_{z'}h$ is of order ϵ , while $\partial_{z'}h$ actually diverges as $z' \rightarrow z'_{tip}$. Indeed, both the asymptotic form of the pressure gradient $(\partial_{z'}h)/h^2$ and of the viscous term $\partial_{z'}[(\partial_{z'}v)h^2]/h^2$ diverge as $h \rightarrow 0$ and $\partial_{z'}h \rightarrow \infty$.

On the other hand, the complete Navier-Stokes problem has no singularities as long as $|t'| > 0$. Surface tension will ensure that the gradient of the curvature remains finite. Hence there is a small region around the tip, whose width goes to zero as $\epsilon \rightarrow 0$, where higher order terms in the Navier-Stokes equation will be important. Its size ℓ_{tip} can be estimated by saying that the asymptotic equations become valid as $\partial_{z'}h$ becomes of order unity at the edge of this region. Thus, since $\partial_{z'}h \approx \ell_r/\ell_{tip}$, we have $\ell_{tip} \approx \ell_r|t'|$, using the known scaling of the radial length scale ℓ_r with $|t'|$.

Now we transform to similarity variables $\xi = z'/|t'|^{1/2}$, where $\xi_{tip} = z'_{tip}/|t'|^{1/2}$ is the position of the tip. Since the width of the tip region shrinks as $|t'|$, it will go to zero like $|t'|^{1/2}$ even in ξ -variables. In the neighborhood of any $\xi \in]\xi_{tip}, \infty[$ the similarity equations will be valid as $|t'| \rightarrow 0$. Thus to capture the leading self-similar behavior of the Navier-Stokes equation after breakup, one just has to find the correct boundary conditions for ϕ and ψ at ξ_{tip} . This situation is reminiscent of the boundary condition at $\xi = \pm\infty$ *before* breakup: For $|t'| \rightarrow 0$ the range of validity of the similarity equations extends to infinity, so supplying boundary conditions at $\xi = \pm\infty$ suffices to uniquely solve the problem.

To derive the correct boundary condition, we proceed as follows: We supplement (18),(19) with higher order terms in ϵ , which regularize the equations at the tip. The corresponding similarity equations in ϕ and ψ now still contain t' as a parameter, but are finite as $\xi \rightarrow \xi_{tip}$. This means solutions of those equations can be supplemented with the natural boundary condition $\phi(\xi_{tip}) = 0$.

Then we derive a simplified version of the equations valid at the tip, which we can integrate explicitly, using $\phi(\xi_{tip}) = 0$ as a boundary condition. Now we can take the limit $|t'| \rightarrow 0$ or $\epsilon \rightarrow 0$, which leaves us with the correct boundary conditions for ϕ and ψ , valid for $t' = 0$. We also show that this result is independent of the particular regularization we have been using, so the result is unique, as expected from the above argument. Once the boundary condition has been found, we can solve the similarity equations to find a unique solution after breakup.

No knowledge of the fluid motion in the tip region of size $\ell_\nu|t'|$ is needed to calculate the self-similar part of the solution. It remains an interesting open problem to devise a method to compute an approximate solution in the tip region. However, since this region becomes arbitrarily small as $|t'| \rightarrow 0$, we will not be concerned with this question in the present paper.

To construct a regularized version of (18), we observe that it can be generalized in the form [23]:

$$\partial_{t'}v + v\partial_{z'}v = -\partial_{z'}p + \frac{\partial_{z'}[(\partial_{z'}v)D^2]}{h^2} \quad , \quad (40)$$

$$\partial_{t'}h + v\partial_{z'}h = -(\partial_{z'}v)h/2 \quad , \quad (41)$$

with

$$p = \frac{1}{2h} \left[\frac{\partial E}{\partial h} - \frac{d}{dz'} \frac{\partial E}{\partial(\partial_{z'}h)} \right] \quad .$$

Here $E = E(h, \partial_{z'}h)$ is a surface energy and $D = D(h, \partial_{z'}h)$ a dissipation kernel. This nomenclature is motivated by the fact that $\partial_{z'}p$ may be written as

$$\partial_{z'}p = \frac{1}{h^2} \frac{d}{dz'} \left[h^2p + (\partial_{z'}h) \frac{\partial E}{\partial(\partial_{z'}h)} - E \right] \quad ,$$

and hence we have the conservation equation

$$\begin{aligned} \frac{\partial}{\partial t'} [h^2v^2/2 + E(h, \partial_{z'}h)] &= -((\partial_{z'}v)D)^2 - \\ \frac{\partial}{\partial z'} \left[(v^2/2 + p)h^2v - v(\partial_{z'}v)D^2 + (\partial_{t'}h) \frac{\partial E}{\partial(\partial_{z'}h)} \right] & \quad . \end{aligned} \quad (42)$$

So apart from a surface term this equation says that the sum of kinetic and potential energy decreases with a negative definite dissipation rate $\mathcal{D} = -((\partial_{z'}v)D)^2$. In the present context, (40),(41) are phenomenological equations. There are certainly other higher order correction terms present in the Navier-Stokes equation, which have not been included. However, the only important point here is that E and D can be chosen such as to make the equations finite at the tip. In [14] we already introduced a variant of (40),(41) with

$$E(h, \partial_{z'}h) = 2h(1 + (\partial_{z'}h)^2)^{1/2} \quad . \quad (43)$$

This energy is proportional to the surface area and arises naturally when keeping the complete curvature term in the boundary condition (4).

If the surface at the tip is non-degenerate and the velocity field is regular, we simply have $h(z, t) = h_0(t)(z' - z'_{tip})^{1/2} + O(z' - z'_{tip})^{3/2}$ and $v(z, t) = v_0(t) + v_1(t)(z' - z'_{tip}) + O(z' - z'_{tip})^2$. As is verified by inspection, the particular form (43) of E succeeds in keeping $\partial_{z'} p$ finite as $z' \rightarrow z'_{tip}$. Introducing

$$D(h, \partial_{z'} h) = h(3/(1 + (\partial_{z'} h)^2))^{1/2} \quad (44)$$

for the dissipation kernel, the same is true for $\partial_{z'}[(\partial_{z'} v)D^2]/h^2$, hence *all* terms in (40) are now finite at the tip. At the same time, the asymptotic equations (18),(19) are recovered for $\epsilon \rightarrow 0$, as this corresponds to

$$\begin{aligned} E_{asympt} &= 2h, \\ D_{asympt} &= \sqrt{3}h. \end{aligned} \quad (45)$$

By construction, all allowed functions E and D must have the same limit (45). We now insert (22) into the regularized equations (40),(41). For $t > t_0$, denoting $|t'|^{1/2}$ by ℓ , we obtain:

$$-\psi/2 - \xi\psi'/2 + \psi\psi' = -G'/\phi^2 + (\psi'D^2)'/\phi^2 \quad (46)$$

and

$$\phi - \xi\phi'/2 + \psi\phi' = -\psi'\phi/2 \quad , \quad (47)$$

where

$$\begin{aligned} G &= -\frac{\phi}{(1 + \ell^2\phi'^2)^{1/2}} - \ell^2 \frac{\phi^2\phi''}{(1 + \ell^2\phi'^2)^{3/2}} \quad , \\ D &= \phi \left(\frac{3}{1 + \ell^2\phi'^2} \right)^{1/2} . \end{aligned} \quad (48)$$

Here for simplicity we have used the special forms (43) and (44) for E and D . For $\ell = 0$ we recover the asymptotic equations (23),(24), while for finite ℓ all terms are regular at the tip as ϕ and ψ behave like

$$\phi \sim (\xi - \xi_{tip})^{1/2} \quad , \quad \psi \sim (\xi - \xi_{tip}) \quad . \quad (49)$$

To focus on the tip region, we introduce the rescaled fields $\bar{\phi}$ and $\bar{\psi}$:

$$\begin{aligned} \bar{\phi}(\zeta) &= \phi(\ell\zeta + \xi_{tip}) \quad , \\ \bar{\psi}(\zeta) &= \ell^{-1}[\psi(\ell\zeta + \xi_{tip}) - \xi_{tip}/2] \quad , \\ \zeta &= \ell^{-1}(\xi - \xi_{tip}) \quad . \end{aligned} \quad (50)$$

In rescaled variables, the equations are

$$\ell^2 \bar{\phi}^2 [-\bar{\psi}/2 - \zeta\bar{\psi}'/2 + \bar{\psi}\bar{\psi}'] - \ell \bar{\phi}^2 \xi_{tip}/4 = \{-\bar{G} + \bar{\psi}'\bar{D}^2\}' \quad , \quad (51)$$

and

$$\bar{\phi} - \zeta\bar{\phi}'/2 + \bar{\psi}\bar{\phi}' = -\bar{\psi}'\bar{\phi}/2 \quad , \quad (52)$$

with

$$\begin{aligned} \bar{G} &= -\frac{\bar{\phi}}{(1 + \bar{\phi}'^2)^{1/2}} - \frac{\bar{\phi}^2\bar{\phi}''}{(1 + \bar{\phi}'^2)^{3/2}} \quad , \\ \bar{D} &= \bar{\phi} \left(\frac{3}{1 + \bar{\phi}'^2} \right)^{1/2} . \end{aligned} \quad (53)$$

In (51)-(53) and (54) below, primes refer to differentiation with respect to the rescaled variable ζ .

The only place where ℓ still appears is in front of the “inertial” terms on the left hand side of (51). This is because any fixed region $\zeta \in [0, \zeta_1]$ near the tip shrinks to zero in ξ -variables as $\ell \rightarrow 0$. But the fluid at the tip should move with the boundary, so it is at rest in the frame of reference of the tip. Indeed, since the left hand side of (51) only contains lower order derivatives, the limit $\ell \rightarrow 0$ is regular at fixed initial conditions for $\bar{\phi}, \bar{\psi}$ at 0.

Hence by putting $\ell = 0$ in (51) we obtain a simplified description of the tip region, which is uniformly valid in any fixed interval $[0, \zeta_1]$. Note that implicitly ℓ is still present by virtue of (50). Solutions of the resulting equations correspond to a very much blown-up version of the tip. Since the solutions are regular at $\zeta = 0$, we can employ the natural boundary condition $\bar{\phi}(0) = 0$, and from (53) we have $\bar{G}(0) = \bar{D}(0) = 0$. This means (51) can be integrated to give

$$\bar{G} = \bar{\psi}' \bar{D}^2 \quad . \quad (54)$$

We now supply appropriate matching conditions, which express the consistency of (52) and (54), valid at the tip, with the solutions outside the tip. At fixed ξ , $\phi(\xi)$ and $\psi(\xi)$ are finite in the limit $\ell \rightarrow 0$. Since the tip region gets arbitrarily small in ξ -variables this is physically reasonable, but has also been checked numerically by integrating (46),(47). Hence we have to require $\bar{\phi}, \bar{\psi}$ to behave like $\bar{\phi}(\zeta) \approx \kappa_1$ and $\bar{\psi}(\zeta)/\zeta \approx \kappa_2$ for large ζ . In view of the scaling (50) this makes them consistent with $\phi(\xi), \psi(\xi)$ finite. Inserting $\bar{\phi}(\zeta) = \kappa_1$ and $\bar{\psi}(\zeta) = \kappa_2 \zeta$ into (52) and (54), one confirms this ansatz to solve the equations, and finds $\kappa_2 = -2$ and $\kappa_1 = 1/6$. So, again considering (50), the lowest order terms of ϕ and ψ as $(\xi - \xi_{tip})$ tends to zero are $\phi = 1/6$ and $\psi = \xi_{tip}/2 - 2(\xi - \xi_{tip})$. In other words, at ξ_{tip} we have the boundary conditions

$$\begin{aligned} \phi(\xi_{tip}) &= 1/6 \quad , \\ \psi(\xi_{tip}) &= \xi_{tip}/2 \quad . \end{aligned} \quad (55)$$

This boundary condition implies that the asymptotic shape of h is a step function of height $|t'|/6$ at the point $z_{tip}(t)$.

It is important to notice that this result is independent of the particular form of regularization (43),(44) we have been using. For example any other term involving h leads to a term $\ell^2 \bar{\phi}$ and drops out as $\ell \rightarrow 0$. Another contribution $\partial_{z'} h$ gives $\bar{\phi}'$ and also does not contribute as we finally set $\bar{\phi} = \kappa_1$.

It only remains to formulate boundary conditions for $\xi \rightarrow \infty$. At large distances from the singular point z_0 both the interface and the velocity field should look the same as before breakup. This is the same reasoning that made us construct solutions which far away from z_0 are static on the time scale of the singularity. As the width of the singular region shrinks to zero like $|t'|^{1/2}$, the large body of fluid outside is not able to follow. Here it provides us with the mechanism for unique continuation: For the two solutions to coincide we must require that

$$\begin{aligned} \lim_{\xi \rightarrow \pm\infty} \phi(\xi)/\xi^2 &= a_0^\pm \quad , \\ \lim_{\xi \rightarrow \pm\infty} \psi(\xi)\xi &= b_0^\pm \quad . \end{aligned} \quad (56)$$

We will see that (55),(56) are all the boundary conditions needed to uniquely solve (23),(24) after breakup. Since the constants a_0 and b_0 are different for the left and right hand side of the problem, the solutions will also differ. In particular, the value of ξ_{tip} consistent with (56) depends on a_0 and b_0 . The requirement (56) thus represents the way the properties of the solution before breakup are communicated to the solution after breakup. Inserting the ansatz

$$\begin{aligned} \phi &= 1/6 + \phi_1(\xi - \xi_{tip})^\alpha + \dots \quad , \\ \psi &= \xi_{tip}/2 - 2(\xi - \xi_{tip}) + e_0(\xi - \xi_{tip})^\beta + \dots \end{aligned} \quad (57)$$

into the similarity equations and balancing leading powers we find $\alpha = 2/5$ and $\beta = 7/5$. We therefore try the general expansion

$$\psi = \xi_{tip}/2 + (\xi - \xi_{tip}) \left[-2 + \sum_{i=0}^{\infty} e_i (\xi - \xi_{tip})^{(2+i)/5} \right] \quad . \quad (58)$$

Again, by (26) it is sufficient to consider the expansion of ψ . The first few coefficients are

$$\begin{aligned}
e_0 &= \frac{60}{7}\phi_1 \quad , \\
e_1 &= 0 \quad , \\
e_2 &= -\frac{120}{7}\phi_1^2 \quad , \\
e_3 &= -\frac{5}{72}\xi_{tip} \quad .
\end{aligned} \tag{59}$$

We confirmed, by deriving recursion relations for the e_i to arbitrarily high order, that all coefficients are determined by the two free parameters ξ_{tip} and ϕ_1 . Since the power series (58) has again a finite radius of convergence, all solutions starting from ξ_{tip} are classified by just two parameters. But for $t > t_0$ the behavior for $|\xi| \rightarrow \infty$ is very different from the situation before breakup. We now have $s = -1$, and according to (33) the asymptotic behavior $\phi \sim \xi^2$, $\psi \sim \xi^{-1}$ is *stable*. So integrating the similarity equations to infinity, for every value of ξ_{tip} and ϕ_1 we will find a unique value of $\lim_{\xi \rightarrow \infty} \phi(\xi)/\xi^2$ and $\lim_{\xi \rightarrow \infty} \psi(\xi)\xi$. Hence the boundary conditions (56) are precisely what is needed to uniquely fix ξ_{tip} and ϕ_1 , and thereby uniquely determining the similarity solution ϕ^- and ψ^- after breakup.

Obviously, this has to be done for the left and right hand sides separately. The left hand side corresponds to a receding neck, the other is the main drop. We denote the values of ξ_{tip} and ϕ_1 by ξ_{neck} and ϕ_{neck} for the left hand side, and ξ_{drop} and ϕ_{drop} for the right hand side. The result of a numerical calculation of ϕ^- and ψ^- can be found in Figure 4, some of the characteristics of the solution are listed in Table 2. Specifically, the neck recedes with the velocity

$$v_{neck} = \frac{\xi_{neck}}{2}|t'|^{-1/2} \quad , \tag{60}$$

where $\xi_{neck}/2 \approx 8.7$. Unfortunately, on the scale of Figure 4 it is hard to see any deviations from a flat interface for the drop. Figure 5 below will give a better idea of how the drop is left distorted after breakup.

It should be appreciated that the unique continuation does not follow from the asymptotic equations (23),(24) alone. Rather, we needed to invoke regularity for $|t'| \neq 0$ to derive the boundary condition $\phi^-(\xi_{tip}) = 1/6$. Indeed, (23) and (24) with $s = -1$ would allow for an infinity of solutions, one for each value of $\phi(\xi_{tip})$.

V. DISCUSSION

We have shown that the motion of a Navier-Stokes fluid close to the time of breakup is described by self-similar solutions. The corresponding scaling functions, before and after the breakup, are solutions to a set of ordinary differential equations. For the solutions to be consistent, both away from the singular point and at the receding tip after breakup, boundary conditions have to be imposed. They lead to unique solutions of the similarity equations. This means solutions to the Navier-Stokes equation close to the singularity are predicted without adjustable parameters, and independent of boundary or initial conditions. It is quite instructive to plot the predicted interface of a real fluid at constant time intervals before and after the singularity. Since ℓ_ν and t_ν are almost on molecular scales for water [14], we take a mixture of glycerol and ethanol as a reference fluid, for which $\ell_\nu = 72\mu m$ and $t_\nu = 114\mu s$. This is large enough for experiments by optical means to be feasible. Measurements of the velocity field are also possible [24]. Figure 5 shows three profiles, each $46\mu s$ apart, before the singularity (a), and after the singularity (b). This corresponds to $|t'| = 1, 0.55$, and 0.1 . In particular, there is no freedom in the spatial scale of this Figure. The same graph should apply regardless of boundary conditions.

Before breakup, one can clearly distinguish a very slender neck, and the steep front of the adjoining drop. As the neck becomes thinner, the minimum moves towards the drop, making the interface even steeper. The greatest relative changes in the diameter occur near the minimum, far away the interface is practically static. As one comes closer to the singularity, the size of the “active” region, which is still changing, becomes smaller and smaller.

After breakup, the neck snaps back very rapidly, forming a sharp front at the end. For $|t'| = 1$, higher order corrections in $|t'|$ will probably be already important, and the end will look more rounded. As seen in Figure 4, there is also some fluid accumulating at the end in the asymptotic solutions, but this cannot be seen on the scale of Figure 5. The small protrusion on the drop, left by the breakup, quickly relaxes to an almost flat interface.

The asymmetry of the breakup was already noticed in experiments [25,26]. However, one must be careful not to apply our results to those experiments directly, since they are on length and time scales $z' \gg 1, |t'| \gg 1$, far away from the asymptotic behavior. Still our similarity solutions could play a crucial role for the shape selection even in this “inviscid” regime, since all solution must ultimately match onto the asymptotic behavior. Clearly, an extension of our theory to the almost inviscid regime seems highly desirable.

Recently, an experimental study of drop formation in a highly viscous fluid has been reported [27]. Qualitatively, the shape of the interface adjoining the primary drop agrees well with Figure 5. Also, the length and time scales of the similarity solution, as given by the present theory, have been used to analyze the data and are found to be consistent with experiment. Unfortunately, at the times shown in Figure 2A and Figure 2B of [27], the straining due to the falling drop is still appreciable compared with the scales of the similarity solution. Also, there is no independent measurement of t' available, which makes a meaningful comparison with theory difficult at present. We will discuss the process of repeated necking, reported in [27], below.

Extensive experiments with high-speed jets, where gravity is irrelevant, are also in progress [28]. The stroboscopic method employed for example in [29] allows to determine t' independently, so comparison with theory can be made without adjustable parameters. Preliminary results show nice agreement with theory before breakup. After breakup a quantitative comparison with theory is not yet possible, due to air drag on the rapidly receding neck, whose effect is not yet included in the equations.

Therefore, we will use numerical simulations for a detailed comparison with theory. In particular, we would like to verify the prediction of the theory that the same similarity solutions are always approached, independent of boundary or initial conditions. Indeed, some simulations have already been performed on the breakup of a Navier-Stokes fluid [30], but they are not sufficiently close enough to the singularity to allow for a meaningful comparison. This is because in the asymptotic region Navier-Stokes computations become prohibitively expensive. To make simulations feasible, one has to resort to approximations.

As model equations, we take the generalized form of the asymptotic equations (40) and (41). Extensive simulations of this system before breakup were already reported in [14], [8], and [27]. The equations read

$$\partial_t v_0 + v_0 \partial_z v_0 = -\frac{\gamma}{\rho} \partial_z p + 3\nu \frac{\partial_z [(\partial_z v_0) H^2]}{H^2} - g \quad , \quad (61)$$

$$\partial_t H + v_0 \partial_z H = -(\partial_z v_0) H / 2 \quad , \quad (62)$$

where

$$p = \frac{1}{H(1 + (\partial_z H)^2)^{1/2}} - \frac{\partial_z^2 H}{(1 + (\partial_z H)^2)^{3/2}} \quad . \quad (63)$$

So apart from the asymptotic terms already contained in (18) and (19), (63) contains the exact expression for the mean curvature of a body of revolution. The system (61)-(63) was supplemented with two types of boundary conditions [14]:

In the “jet geometry” we fix the values of H and v_0 at two fixed points z_+ and z_- :

$$H(z_{\pm}, t) = H_{\pm}(t) \quad , \quad (64)$$

$$v_0(z_{\pm}, t) = v_{\pm}(t) \quad . \quad (65)$$

Hence here we envision a jet of length $z_+ - z_-$ with nozzle radius $H_+ = H_- \equiv r_0$ and speed $v_+ = v_- \equiv V$. At some point in time a small perturbation is applied to the speed v_- at the nozzle and the jet breaks up according to the Rayleigh instability. The jet speed is so high that gravitational effects can be neglected, and thus $g = 0$.

In the “drop geometry” fluid is released slowly from a tap. Thus at the opening of the tap, z_- say, boundary conditions (64) and (65) hold, while at the lower end of the drop the boundary moves with the fluid. This means we have

$$H(z_+(t), t) = 0 \quad (66)$$

and

$$v_0(z_+(t), t) = \partial_t z_+(t) \quad . \quad (67)$$

In this experimental situation gravity is of course important, as initially gravitational and surface tension forces are balanced, and the drop assumes an equilibrium shape [31]. These shapes are reproduced exactly by the stationary solutions of (61)-(63). Eventually, gravity overcomes surface tension and the drop falls and subsequently pinches off.

The implementation of boundary conditions as well as the numerical procedure is explained in detail in [14]. In [14] and [27] simulations of (61)-(63) have been used to reproduce experimental interface shapes both for high and

low viscosity fluids in different geometries. In particular in the case of a slowly dripping tap [26], both boundary and initial conditions are known and comparison with experiment can be done without adjustable parameters. Thus the excellent agreement between simulation and the experimental shape of a falling drop at the pinch point [14] seems highly significant. Therefore we are confident that (61)-(63) represents a good approximation to the Navier-Stokes equation not only close to the pinch point, but also for earlier times and including the crossover to the boundary.

We have performed systematic tests of the predictions of the present theory, in particular investigating the independence of the singular behavior near break-off from boundary conditions. For all runs, both in the jet and the drop geometry, and independent of the nozzle or tap diameter and of the viscosity, we always found the flow to converge onto the similarity solution predicted by the present theory.

Figure 6 shows this convergence for a typical run in the jet geometry. The nozzle diameter is 100 in units of ℓ_ν . The solution near the singularity has been converted to similarity variables, thus giving $\phi(\xi)$ and $\psi(\xi)$ using the transformation (22). Shown is the predicted similarity solution as a solid line, and the computed solution at times $|t'| = 0.39, 0.13, 0.043$, and 0.014 , represented by dashed, chain-dashed, dot-dashed, and dotted lines. It can clearly be seen that the range of validity of the similarity solution *expands* like $|t'|^{-1/2}$ in the similarity variable ξ . This means there is a *fixed* region in z' where the similarity theory applies, in agreement with the statements of Section 3. At the boundary of this region, the slope $\partial_z h$ becomes of order unity, and the expansion in orders of ϵ breaks down.

The motion shown in Figure 6 occurs on scales widely separated from those imposed by the boundary conditions. The time distance from the onset of the linear instability to the singularity is $t_0/t_\nu = 32284$, much larger than the relevant t' . Similarly, the nozzle diameter, converted to the similarity variable ξ , is $\xi = 157, 272, 473$, and 829 , for the times shown. Clearly the motion near the singularity has become independent of these imposed length and time scales. The same will happen for *any* boundary condition, as both the typical time and length scale shrinks to zero near the singularity.

Next we test the convergence onto the similarity solution after breakup. Since there is a moving tip, we modify the viscous term in (61) to regularize the tip. The force balance now reads

$$\partial_t v_0 + v_0 \partial_z v_0 = -\frac{\gamma}{\rho} \partial_z p + 3\nu \frac{\partial_z [(\partial_z v_0) H^2 / (1 + a(\partial_z H)^2)]}{H^2} - g \quad , \quad (68)$$

where a is a free constant. By varying a we can test our prediction that the shape of the interface after breakup does not depend on the regularization employed.

To produce an initial condition after breakup, we take a simulation before breakup, which has progressed to a time distance of $|t'| = 10^{-4}$ from the singularity. Then we cut the solution at the minimum and interpolate H to zero with a polynomial, so as to keep the highest derivatives smooth. This we take as the new initial condition after breakup and let the solution evolve under (68), (62), and (63). For a wide range of values of a in (68), we always find the solution to converge onto the similarity form found in Section 4. Figure 7 illustrates this convergence for a run which has the same boundary conditions and material parameters as the one shown in Figure 6 before breakup. The constant a was chosen to be 1. Again, solutions were converted to similarity variables. The full line represents the predicted similarity solution, the dot-dashed and the dashed lines show the numerical simulations for $|t'| = 0.006$ and $|t'| = 0.06$ after the singularity. The dotted line is the similarity solution before breakup, shown for comparison. It can clearly be seen that after the solution has been cut in two halves it rapidly converges onto the predicted similarity form. This is independent of both the regularizing term in (68) and the procedure by which the solution is cut.

Hence both before and after the singularity, we have always observed convergence onto the similarity solutions if $|t'|$ is small. Still it would be very useful to have a better mathematical understanding of the approach of the similarity solution for the full Navier-Stokes dynamics. Even for the simplified model equations (61)-(63) the convergence we found numerically is far from being a trivial result, as there are higher order derivative terms like $\partial_z^3 H$ coming from the pressure. In principle, although these terms are multiplied by a small number t' close to the singularity, they could make a singular perturbation, which changes the asymptotics. However, it is well beyond the scope of this paper to explore these questions in detail, so at present we have to rely on the ample numerical evidence.

Another important question is the stability of the similarity solution to small perturbations. This has been studied in the framework of the asymptotic equations (18),(19) in [32], both numerically and analytically. The result is that the similarity solutions are linearly stable as expected, since there are observed numerically. On the other hand, they are unstable to *finite amplitude perturbations* of wavelength comparable to the minimum radius of the fluid neck.

As soon as a perturbation is large enough, it will start to grow and eventually forms a new similarity solution with its own z_0 and t_0 . For any finite number of such perturbations, the singularities are separated in space and the present theory strictly applies. However, if one explicitly adds an external white noise source to the Navier-Stokes equation, perturbations are introduced on all time scales arbitrarily close to the singularity. This allows for the appearance of a “rough” interface as described in [27] and [32], consisting of an infinity of interacting similarity solutions. Locally, the form of each of those solutions, seen as “necks” in experiment, is consistent with the present theory.

In [32], a threshold length scale

$$\ell_{thres} \sim \ell_\nu \left(\frac{\ell_T}{\ell_\nu} \right)^{2/5} \quad (69)$$

was identified, below which thermal fluctuations become important. The relevant thermal length scale for surface perturbations is $\ell_T = (k_B T / \gamma)^{1/2}$. For a mixture of 85% glycerol and 15% water ℓ_{thres} is $1 \mu m$. Thus, in the presence of thermal fluctuations, the microscopic length scale ℓ_{micro} introduced in Section 3 may be replaced by ℓ_{thres} : for H_{min} larger than ℓ_{thres} the Navier-Stokes equation is applicable, on smaller scales the equations are inherently stochastic.

An obvious benefit one expects from the universality found in the present paper is the unique continuation of Navier-Stokes *simulations* through the singularity. One slight problem lies in the nonanalyticity of ϕ^- and ψ^- if one wants to use similarity solutions as new initial conditions after breakup. Although the pressure itself would be finite, pressure gradients and the viscous term would be infinite at the tip. Thus it is better to use regularized similarity functions, where a small but finite cut-off parameter ℓ has been introduced. The resulting initial conditions for the new Navier-Stokes problem after the singularity would be arbitrarily close to the similarity form, but still finite at the tip.

In conclusion, we have shown that the Navier-Stokes equation carries us through the bifurcation point where at first it seems meaningless. As usual, classical hydrodynamic theory has a much wider range of applicability than purely microscopic considerations would tell us.

ACKNOWLEDGMENTS

I am grateful to a great number of people, for discussions and all sorts of help and encouragement. In particular Hartwig Brand, Michael Brenner, Todd Dupont, Greg Forest, Siegfried Grossmann, Leo Kadanoff, Michael Tabor, and Stephane Zaleski.

-
- [1] P. S. de Laplace, *Mécanique Celeste*, Supplement au X Livre (Courcier, Paris, 1805).
 - [2] F. Savart, “Mémoire sur la Constitution des Veines liquid lancées par des orifices circulaires en mince paroi,” *Ann. Chim.* **53**, 337 (1833).
 - [3] G. Hagen, “Über die Auflösung flüssiger Cylinder in Tropfen,” *Verhandlungen Preuss. Akad. Wissenschaften*, p.281, (Berlin, 1849).
 - [4] Lord Rayleigh, “On the instability of jets,” *Proc. London Math. Soc.* **4**, 10 (1878).
 - [5] C. Weber, “Zum Zerfall eines Flüssigkeitsstrahles,” *ZAMM* **11**, 136 (1931).
 - [6] S. Grossmann and A. Müller, “Instabilities and Decay Rates of Charged Viscous Liquid Jets,” *Z. Phys. B* **57**, 161 (1984).
 - [7] K. C. Chaudhary and L. G. Redekopp, “The nonlinear instability of a liquid jet,” Part 1: Theory, *J. Fluid Mech.* **96**, 257 (1980).
 - [8] J. Eggers, “Universal Pinching of 3D Axisymmetric Free-Surface Flow,” *Phys. Rev. Lett.* **71**, 3458 (1993).
 - [9] R. E. Goldstein, A. I. Pesci, and M. J. Shelley, “Topology Transitions and Singularities in Viscous Flows,” *Phys. Rev. Lett.* **70**, 3043 (1993).
 - [10] M. Tjahjadi, H. A. Stone, and J. M. Ottino, “Satellite and subsatellite formation in capillary breakup,” *J. Fluid Mech.* **243**, 297 (1992).
 - [11] B. Lafaurie, C. Nardone, R. Scardovelli, S. Zaleski, and G. Zanetti “Modelling merging and fragmentation in multiphase flows with SURFER,” *J. Comp. Phys.* **113**, 134 (1994).
 - [12] P. Constantin, T. F. Dupont, R. E. Goldstein, L. P. Kadanoff, M. J. Shelley, and S. M. Zhou, “Droplet breakup in a model of the Hele-Shaw cell,” *Phys. Rev. E* **47**, 4169 (1993).
 - [13] S. E. Bechtel, M. G. Forest, and K. J. Lin, “Closure to all orders in 1-D models for slender viscoelastic free jets: An integrated theory for axisymmetric, torsionless flows,” *SAACM* **2**, 59 (1992).
 - [14] J. Eggers and T. F. Dupont, “Drop Formation in a One-Dimensional Approximation of the Navier-Stokes Equation,” *J. Fluid Mech.* **262**, 205 (1994).
 - [15] L. D. Landau and E. M. Lifshitz, *Fluid Mechanics*, (Pergamon, Oxford, 1984).
 - [16] M. G. Forest, private communication (1994).
 - [17] D. B. Boggy, “Drop Formation in a circular liquid jet,” *Ann. Rev. Fluid Mech.* **11**, 207 (1979).
 - [18] J. B. Keller and M. J. Miksis, “Surface Tension Driven Flows,” *SIAM J. Appl. Math.* **43**, 268 (1983).

- [19] A. L. Bertozzi, M. P. Brenner, T. F. Dupont, and L. P. Kadanoff, “Singularities and Similarities in Interface Flow,” in: L. Sirovich, Editor, Trends and Perspectives in Applied Mathematics, Applied Mathematics Series, Vol. 100, Springer Verlag, N. Y. (1994).
- [20] I am grateful to Jens Hoppe for pointing this out to me.
- [21] C. M. Bender and S. A. Orszag, *Advanced mathematical methods for scientists and engineers*, (Mc Graw-Hill, N. Y., 1978).
- [22] R. A. London and B. P. Flannery, “Hydrodynamics of X-Ray Induced Stellar Winds,” *Astrophysical Journal* **258**, 260 (1982).
- [23] This generalization is due to Peter Constantin.
- [24] E. Marschall, “Zur Strömungsmechanik während der Tropfenbildung in flüssigen Zweiphasen,” *Ver. Deutscher Ingen. Forschungsheft* **632**, 13 (1985).
- [25] E. F. Goedde and M. C. Yuen, “Experiments on liquid jet instability,” *J. Fluid Mech.* **40**, 495 (1970).
- [26] D. H. Peregrine, G. Shoker, and A. Symon, “The bifurcation of liquid bridges,” *J. Fluid Mech.* **212**, 25 (1990).
- [27] X. D. Shi, M. P. Brenner, and S. R. Nagel, “A Cascade Structure in a Drop Falling from a Faucet,” *Science* **265**, 157, (1994)
- [28] T. A. Kowalewski, “Experiments on the late stages of drop formation,” unpublished.
- [29] E. Becker, W. J. Hiller, and T. A. Kowalewski, “Experimental and theoretical investigation of large-amplitude oscillations of liquid droplets,” *J. Fluid Mech.* **231**, 189 (1991).
- [30] F. Shokoohi and H. G. Elrod, “Algorithms for Eulerian Treatment of Jet Breakup Induced by Surface Tension,” *J. Comput. Phys.* **89**, 483 (1990).
- [31] D. H. Michael and P. G. Williams, “The equilibrium and stability of axisymmetric pendant drops,” *Proc. R. Soc. London A* **351**, 117, (1976).
- [32] M. P. Brenner, X. D. Shi, and S. R. Nagel, “Nonsteady Droplet Breakup,” *Phys. Rev. Lett.*, to appear (1994).

ξ_0	ϕ_0	ξ_{min}	ϕ_{min}	ψ_{max}	a_0^+	b_0^+	a_0^-	b_0^-
-1.5699	0.030432	-1.6024	0.030426	-3.066	4.635	0.0723	6.047×10^{-4}	57.043

TABLE I. Some characteristics of the similarity functions ϕ^+, ψ^+ before breakup. The symbols ξ_0 and ϕ_0 stand for the position of the stagnation point, where the fluid is at rest in the frame of reference of the interface, and the radius of the interface at that point. The minimum value of ϕ^+ is ϕ_{min} , and ξ_{min} is its position. The function ψ^+ reaches a maximum value of ψ_{max} . The numbers a_0^\pm and b_0^\pm stand for the limits $\lim_{\xi \rightarrow \pm\infty} \phi^+(\xi)/\xi^2$ and $\lim_{\xi \rightarrow \pm\infty} \psi^+(\xi)\xi$, respectively. All numbers are accurate to the decimal places shown.

ξ_{neck}	ϕ_{neck}	ξ_{drop}	ϕ_{drop}
17.452	0.06183	0.4476	0.6180

TABLE II. Characteristics of the similarity functions ϕ^-, ψ^- after breakup. The tip position of the left hand, or neck side is ξ_{neck} , and the expansion coefficient ϕ_1 , cf. (57), is ϕ_{neck} . Correspondingly, ξ_{drop} and ϕ_{drop} uniquely determine the “drop” side of ϕ^- and ψ^- . The values of a_0^\pm and b_0^\pm are the same as before breakup, cf. Table 1.

FIG. 1. A sketch of the flow geometry investigated in the present paper. The radius or “height” of the free surface at a point z on the axis of symmetry is $H(z)$. The velocity field inside the fluid is $\mathbf{v}(z, r) = v_z(z, r)\mathbf{e}_z + v_r(z, r)\mathbf{e}_r$.

FIG. 2. A plot of the similarity functions ϕ^+ , (a), and ψ^+ , (b), before breakup. Note the strong asymmetry.

FIG. 3. A cartoon of a receding tip after breakup. The position of the tip is $z'_{tip}(t)$.

FIG. 4. The similarity functions ϕ^- , (a), and ψ^- , (b), which are unique continuations of ϕ^+ and ψ^+ to times greater than t_0 . The asymptotic behavior for $\xi \rightarrow \pm\infty$ is by definition the same as before breakup. On the left is the rapidly receding “neck” part of the solution, on the other side is the drop. The points at ξ_{neck} and ξ_{drop} , from where the interface is plane, are marked by diamonds.

FIG. 5. The breakup of a mixture of 5 parts of glycerol in 4 parts of ethanol, as calculated from the similarity solutions. Part (a) shows three profiles before breakup, in time distances of $46\mu s$, corresponding to $|t'| = 1, 0.55$, and 0.1 . In part (b) the same is shown after breakup.

FIG. 6. Simulation of (61)-(63) in the jet geometry. The profiles close to pinch-off were converted to similarity variables. The full line is the prediction of the present theory; the dashed, chain-dashed, dot-dashed, and dotted lines represent the simulation at $|t'| = 0.39, 0.13, 0.043$, and 0.014 . The inset contains a blowup of the central region with only the latest time, $|t'| = 0.014$.

FIG. 7. The approach of the similarity function ϕ^- by the solution of (68),(62) and (63) in the jet geometry, transformed to similarity variables. The fluid neck is severed at $|t'| = 10^{-4}$ before breakup. The full line is ϕ^- , the dotted line the solution before breakup. The dot-dashed and the dashed lines show the simulation at $|t'| = 0.006$ and $|t'| = 0.06$, respectively.

Figure 1:

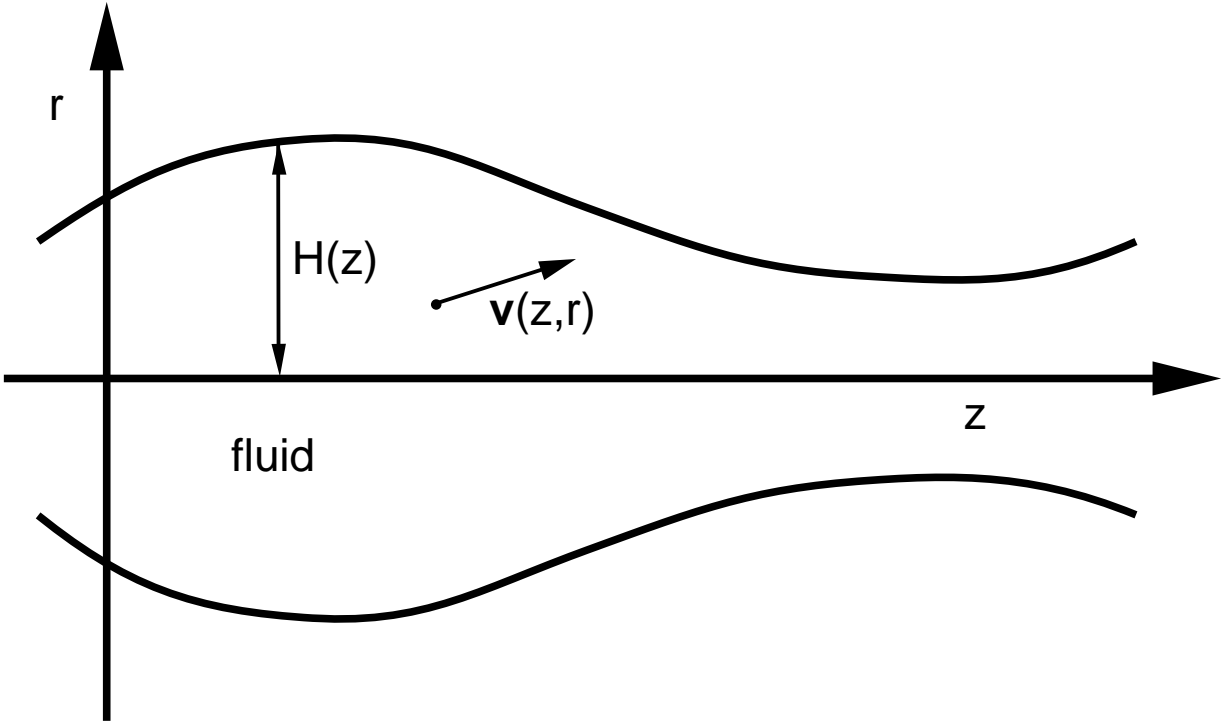


Figure 2a:

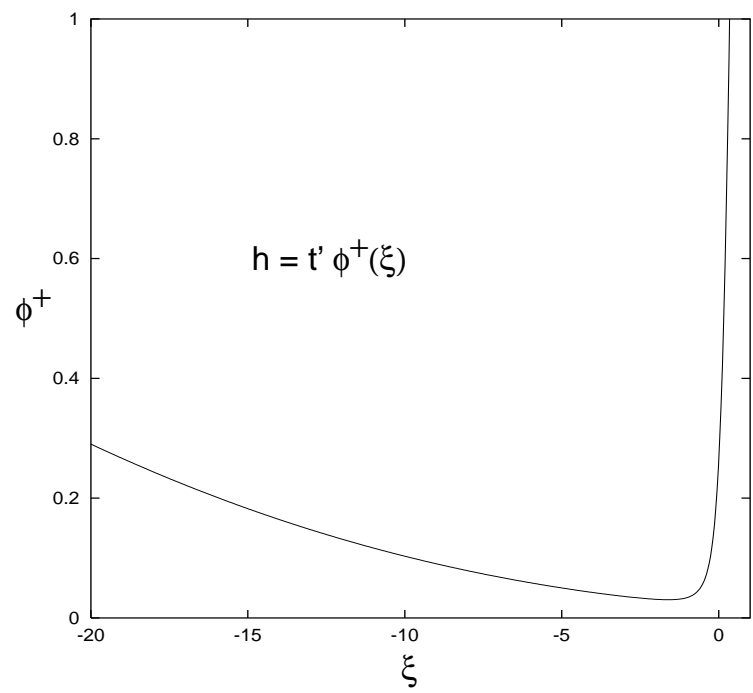


Figure 2b:

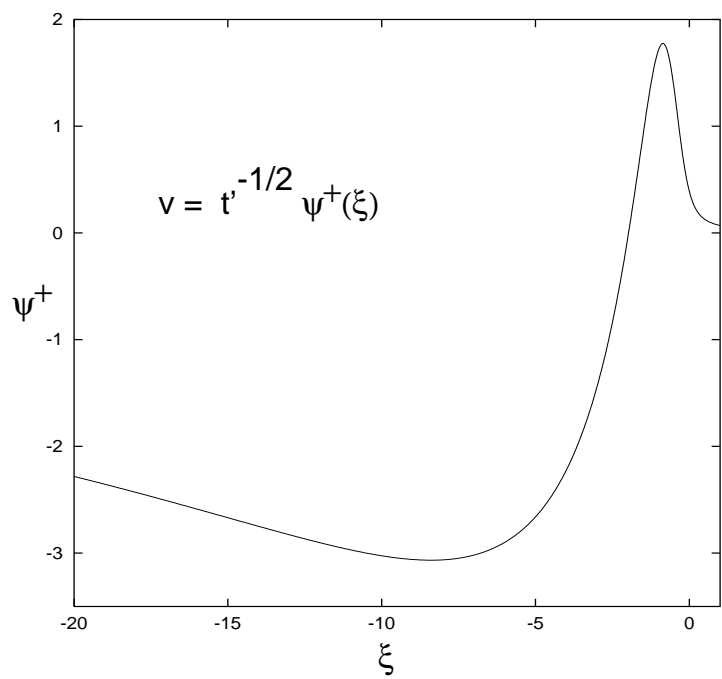


Figure 3:

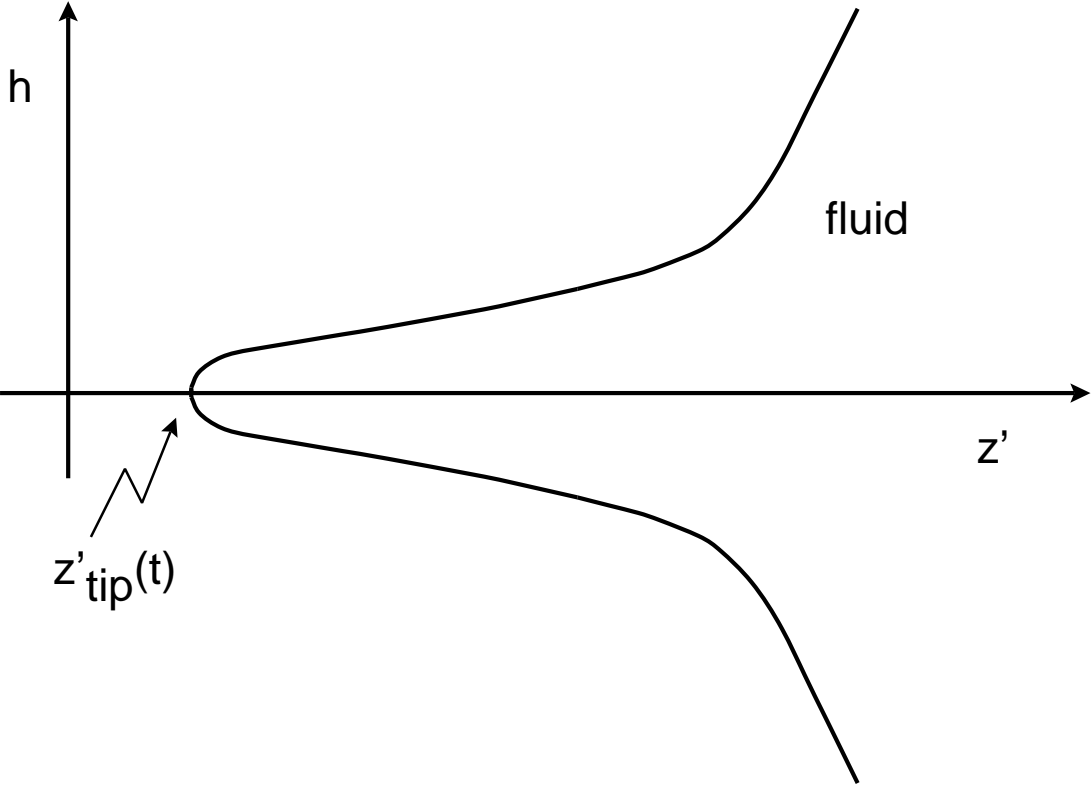


Figure 4a:

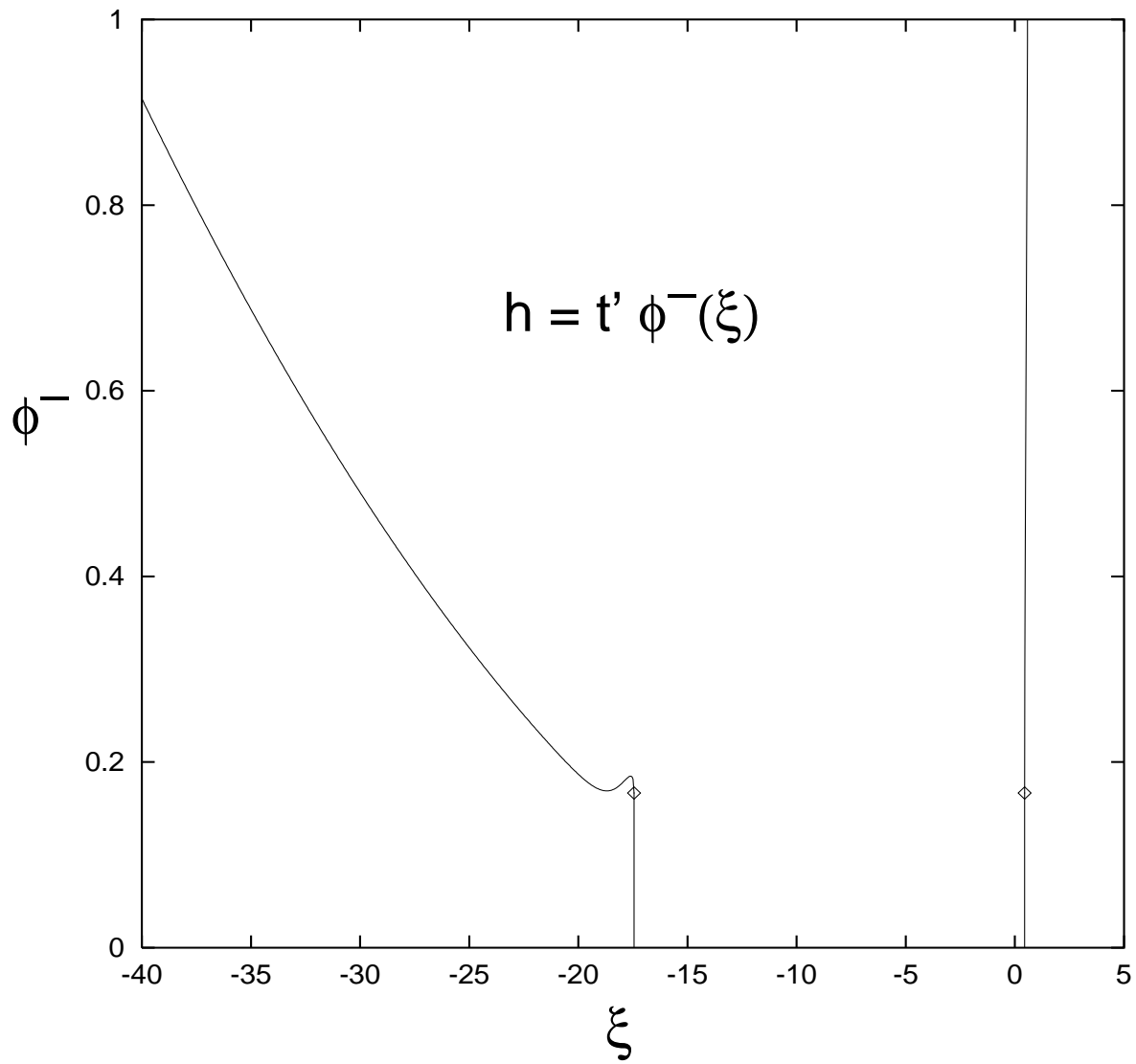


Figure 4b:

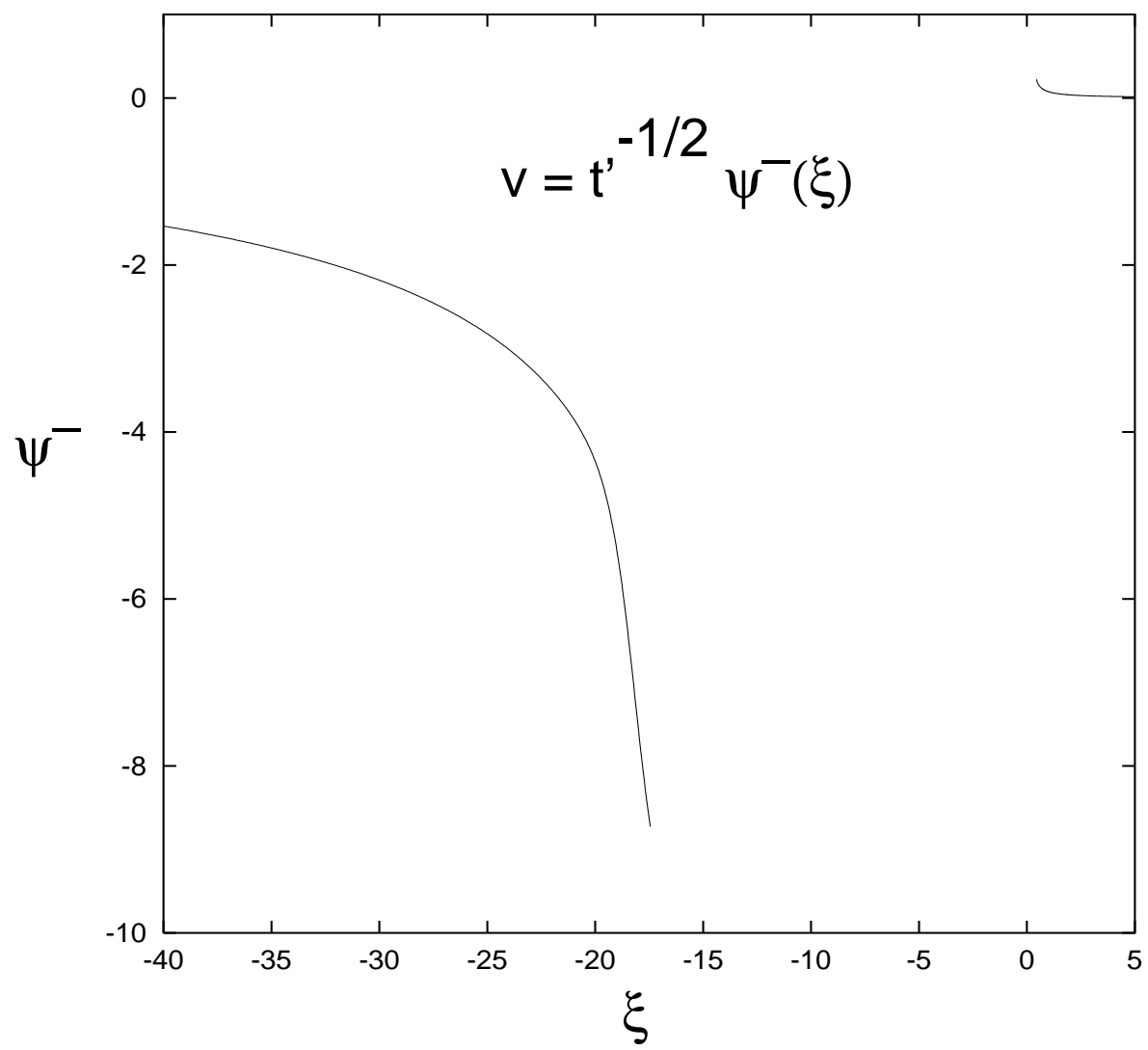


Figure 5a:

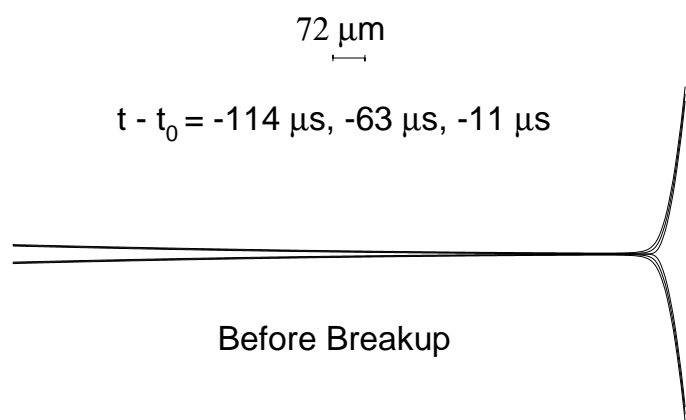


Figure 5b:

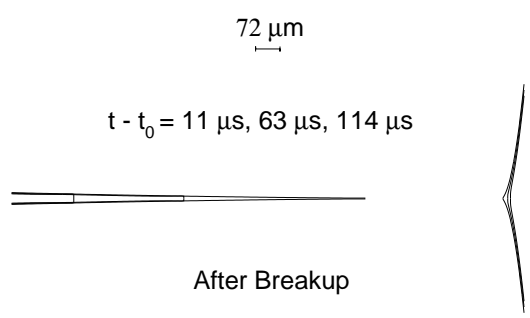


Figure 6a:

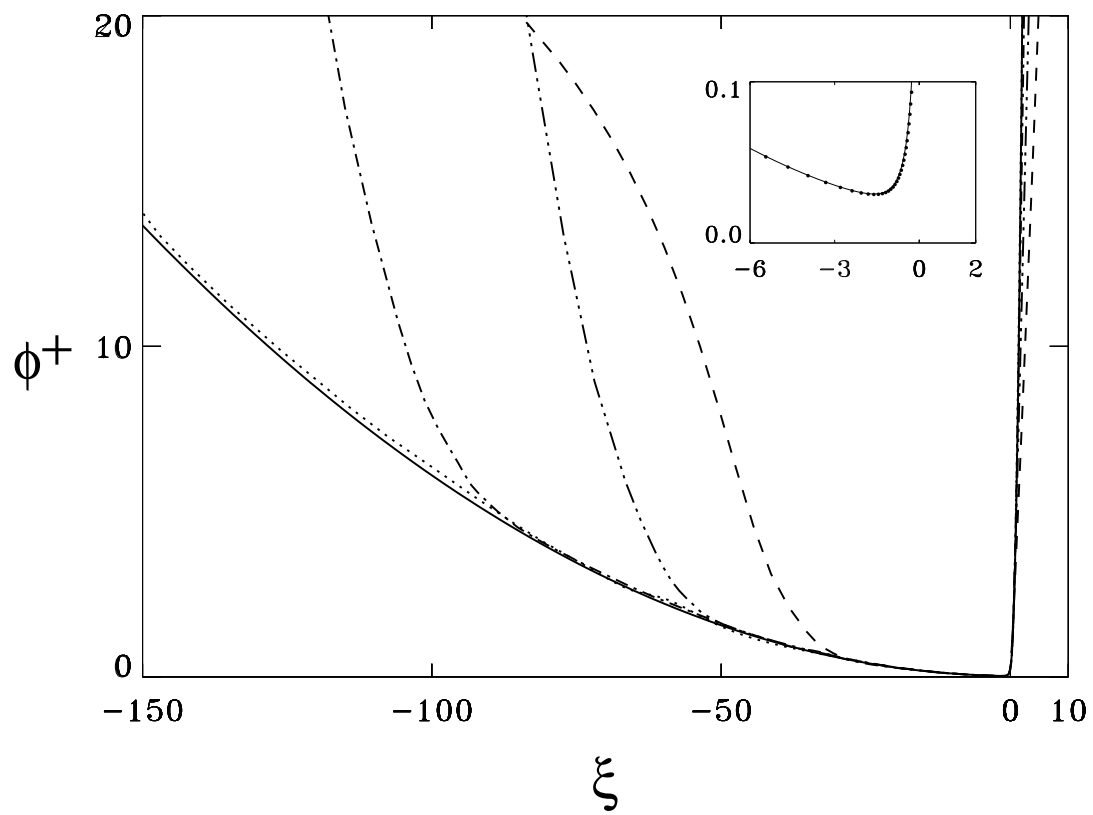


Figure 6b:

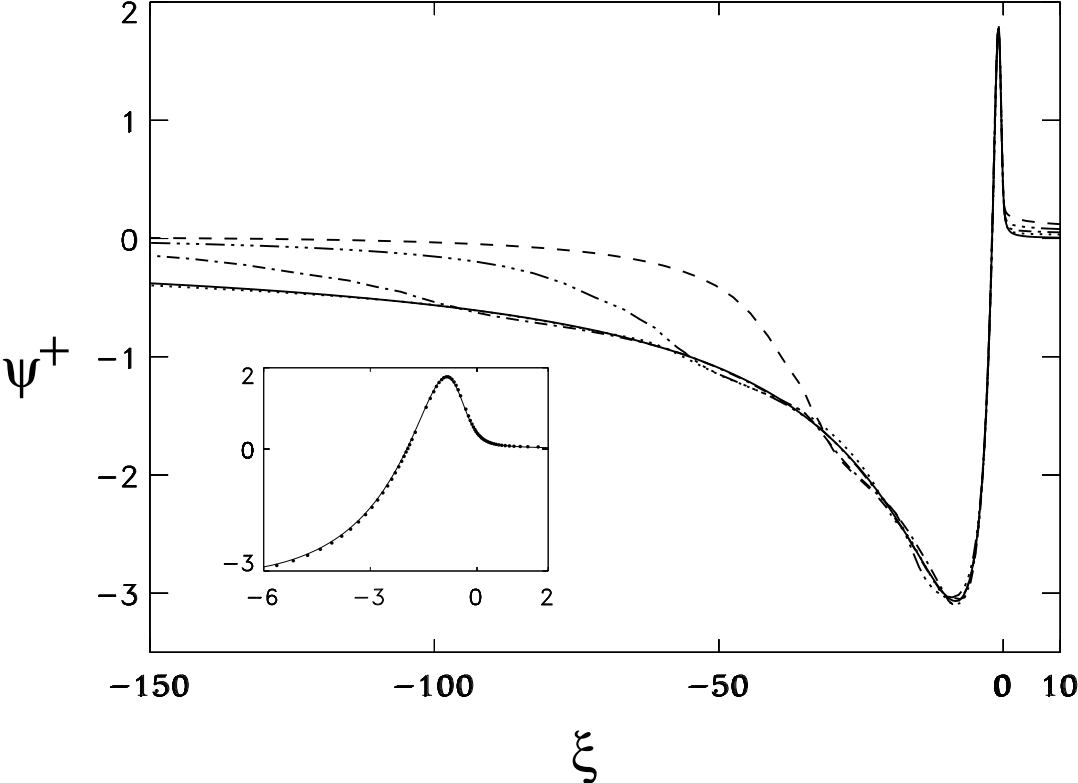


Figure 7:

